Comparison of 2D and 3D prediction models for environmental vibration induced by underground railway with two types of tracks

Qingyuan Xu [a, b, c], Zucai Xiao [a], Tao Liu[d], Ping Lou[a b, c*], and Xuming Song [a]

a. *School of Civil Engineering, Railway Campus, Central South University, 22 Shao-shan-nan Road, Changsha, Hunan 410075, China.*

b. *Key Laboratory of Heavy Railway Engineering Structure of Education Ministry, Railway Campus, Central South University, 22 Shao-shan-nan Road, Changsha, Hunan 410075, China.*

c. *Collaborative Innovation Center of Rail Safety, Central South University, 22 Shao-shan-nan Road, Changsha, Hunan 410075, China.*

d. *School of Civil Engineering, University of Nottingham, University Park, Nottingham, NG7 2RD, UK*

Abstract:

Two-dimensional (2D) and three-dimensional (3D) prediction models for environmental vibration induced by underground railway with direct fixation track and steel spring floating slab track are developed and verified. The responses of ground surface calculated by 2D prediction models with various equivalent forces are compared to those calculated by 3D prediction models. The numerical results show that (a) the computational time for each case calculated by 2D prediction models is more than 500 times less than that calculated by 3D prediction models, however, the accuracy of 2D prediction models is relatively lower than 3D prediction models, so 3D prediction models are required for absolute prediction due to their higher accuracy and applicability to a wider range of complex problems; and (b) a suitable equivalent force transfer method for 2D prediction models can improve the prediction accuracy of 2D prediction models, the equivalent forces in 2D prediction models are respectively recommended to use the equivalent wheel-rail force and the equivalent steel spring force averaged over a vehicle length for underground direct fixation track and steel spring floating slab track.

Keywords:

Environmental vibration, Subway train, Tunnel, Railway engineering, Three-dimensional models, Two-dimensional models.

1 Introduction

With the rapid growth of population in metropolitan areas, underground railways are widely used to relieve the ground transportation pressure in big cities all around the world. However, vibrations induced by underground railway propagate through the tunnel and surrounding soil into nearby buildings. At some locations, these vibrations may reach an intolerable level. Numerical prediction models, which complement analytical models, field measurements and empirical prediction models, are required to assess underground train-induced environmental vibration and to study the valid vibration-reduction countermeasures to be taken. In recent years, great efforts have been made to develop numerical prediction models to deal with these problems.

Two-dimensional (2D) prediction models, which consider only a 2D profile of the three-dimensional (3D) track-tunnel-soil models perpendicular to the railway line, are widely used for the prediction of environmental vibration due to underground railway. For example, Chua et al. [1] developed a 2D finite-element model to calculate the dynamic responses of the subway-soil-structure interaction problem. Tadeu et al. [2] used boundary element method (BEM) to study the 2D wave field generated by buried structures of arbitrary shape in an elastic medium illuminated by dynamic line sources. Yang et al. [3] developed a 2D tunnel-soil foundation interaction model using finite and infinite elements. Nejati et al. [4-5] developed a 2D finite difference prediction model to study the environmental vibration problem. Jones and Hunt [6] developed a 2D prediction model using thin-layer method to simulate semi-infinite layered soil. Godinho et al. [7] presented a frequency domain coupled model making use of the finite element method (FEM) and the method of fundamental solutions to address soil-structure interaction problems. Sun et al. [8] used a 2D finite element model with combination of elastic damping boundary and boundary large elements to study the influence of vibration induced by metro trains on sensitive instruments and corresponding mitigation measures. Huang and Shi [9] analyzed the attenuation zones of a 2D infinite periodic pile barrier subjected to plane waves by plane wave expansion method.

The 2D analysis is attractive due to its computational efficiency. However, the problem of train-track-tunnel-soil is 3D by nature. The results calculated with the 2D prediction models are approximate and qualitative in nature. Considering the fact that 3D responses can be obtained from the

2D profile by the Fourier transform technique or Floquet transform technique by assuming the invariance or periodic of track-tunnel-soil system along the train-moving direction. Many researchers use Fourier or Floquet transform method to study environmental vibration for their relative efficiency and accuracy.

Yang and Hung [10] proposed a so-called two-and-a-half dimensional (2.5D) finite/infinite-element approach by using the Fourier transform of the coordinate in the train-moving direction for modeling the viscoelastic bodies subjected to moving loads. And influence of some parameters of soil, tunnel and train on the environmental vibration due to underground traffic was investigated [11]. More recently, Hung et al. [12] incorporated the track irregularity and dynamic properties of the moving train in the 2.5D prediction model to study the effect of track irregularity on environmental vibration.

Sheng et al. [13] and François et al. [14] developed 2.5D finite/boundary element method in the transformed wave-number domain for studying the train-induced vibrations. Galvin et al. [15] compared the method with the Pipe in Pipe method developed by Hussein and Hunt [16].

Müller et al. [17] proposed a similar approach by coupling the finite element and integral transform methods in the transformed wave-number domain to study the problem of vehicle-slab track-tunnel-soil interaction.

Bian et al. [18] developed a 2.5D finite element track-tunnel-soil interaction model under moving train. The novelty of the model is that gradually damped artificial boundary which can efficiently simulate the wave propagation in the infinitely extended ground was adopted in the model.

Degrande et al. [19] proposed a coupled finite/boundary element model by using the Floquet transform method assuming the geometry to be periodic instead of invariant in the track direction. Chebli et al. [20] illustrated the versatility of the proposed model. Gupta et al. [21-23] used the model to study the influence of some tunnel and soil parameters on the responses of ground surface, to assess the vibration isolation efficiency of continuous and discontinuous floating slab tracks, and to predict the vibrations induced by underground railway traffic in Beijing.

Enhanced by the advent of high-performance computers and the development of rapid solution technique for large-scale sparse equations, 3D prediction models for environmental vibration are now widely used by many researchers.

Wolf [24] used a 3D finite-difference model to evaluate the impacts of low frequency ground vibration (<6.3 Hz) from underground light rail system on the vibration sensitive test equipment of laboratories of the University of Washington. Ma et al. [25] developed a 3D track-tunnel-soil-building finite element model to analyze the vibrations of buildings. Gardien and Stuit [26] presented a finite element modular model, which consisted of three sub-models, namely, the static 3D deflection model, the 2D track model and the 3D propagation model, to analyze vibrations generated by a train travelling in a tunnel. Yaseri et al. [27] developed a 3D coupled scaled boundary finite-element/finite-element method to study the ground vibrations induced by underground trains. Saitoh and Hirose [28] developed a coupled 2.5D and 3D boundary element method to study the influence of a pile on ground vibrations induced by a moving train in an underground tunnel.

From the reviews above, it can be seen that great efforts have been made on the study of various prediction models for environmental vibration induced by underground railway traffic. However, few research works were made on the comparison of 2D and 3D approaches and the applicability of 2D approaches. In order to study the similarity and difference between 2D and 3D responses, as well as to assess the applicability of 2D approach, Andersen and Jones [29] made some comparative studies on the 2D and 3D responses of ground surface due to underground traffic. However, there are still some limitations in their work. On the one hand, their work was based on the frequency domain where harmonic loads instead of practical loads with various frequencies were used. On the other hand, the track, which has significant influence on the environmental vibration, was not included in their model.

The laws of similarity and difference of ground surface responses calculated by various 2D and 3D prediction models for different types of underground track structures vary greatly. In order to help people have a deeper understanding on the similarity and difference of responses of ground surface calculated by various 2D and 3D prediction models for different types of underground track structures, and to help people have a deeper understanding on the applicability of various 2D prediction models for environmental vibration for different underground track structures. In this paper, a comparative study on responses of ground surface, which are calculated by various 2D and 3D prediction models for environmental vibration due to subway train running on direct fixation track and steel spring floating slab track with track irregularity, is conducted in detail in time domain.

One novelty and contribution of this paper is that subway train- mixed 2D and 3D ballastless

track-tunnel-soil coupling dynamic models, which consider the moving train along the track with both medium-long and short wavelength track irregularity, consider the coupling effect among subway train, ballastless track, tunnel and soil, and can reduce the 3D computational time, are developed and used to study the 3D responses of the ground surface. Another novelty and contribution is that responses of ground surface calculated by 2D prediction models with various equivalent forces are compared to those calculated by 3D prediction models for underground direct fixation track and underground steel spring floating slab track in time domain. At last, suggestions for the suitable equivalent forces for 2D prediction models which can improve the prediction accuracy of environmental vibration for underground direct fixation track and underground steel spring floating slab track are given.

2 Models description

Two types of models, namely, 2D and 3D prediction models, are used respectively for prediction of 2D and 3D environmental vibration for underground railway with two types of tracks.

2.1 2D prediction models

2D prediction models consist of two sub-models, namely, 2D load generation sub-models and 2D wave propagation sub-models. 2D load generation sub-models are combined with 2D wave propagation sub-models to calculate the vibration responses of ground surface. Firstly, 2D load generation sub-models are used to obtain the wheel-rail forces, the fastening forces or the steel spring forces. Then, the forces are averaged according to various equivalent force transfer methods first and used later in the 2D wave propagation sub-models to study the 2D responses of the ground surface. The two sub-models are introduced as follows.

2.1.1 2D load generation sub-models

Two types of 2D Load generation sub-models are considered, namely, 2D load generation sub-models for underground direct fixation track and steel spring floating slab track, which are shown in Fig. 1(a) and Fig. 1(b) respectively.

In Fig. 1(a) and Fig. 1(b), a subway train consisting of a series of identical 4-wheel vehicles moves along the underground direct fixation and steel spring floating slab track with random track irregularity at a constant speed v respectively.

Each vehicle in Fig. 1 is modeled as a mass-spring-damper system consisting of a car body with

vertical and pitch motions, two bogie frames with vertical and pitch motions, four wheels with vertical motion, and two-stage suspensions.

The rail, slab, and tunnel in Fig. 1(a) and Fig. 1(b) are simulated by 2D Bernoulli-Euler beam elements. The fastener and the tunnel foundation in Fig. 1(a) and Fig. 1(b) are, respectively, simulated by discrete and continuous linear spring-damper elements, the mat layer for direct fixation track in Fig. 1(a) is simulated by continuous linear spring-damper element, the steel spring and the shear hinge for steel spring floating slab track in Fig. 1(b) are simulated by discrete linear spring-damper elements.

The interaction elements between the moving wheels and the rails, and the track irregularity in Fig. 1 will be described in detail in Section 2.3 and Section 2.4 below respectively.

2.1.2 2D wave propagation sub-models

The schematic of the 2D wave propagation sub-models is shown in Fig. 2. If the acting force $P(t)$ is the averaged wheel-rail force or averaged fastening force, then the sub-model in Fig. 2(a), which consists of slab, mat layer, tunnel and soil, will be used. If the acting force $P(t)$ is the averaged steel-spring force, then the sub-model in Fig. 2(c), which only consists of tunnel and soil , will be used.

Except that two tunnel elements near the track (Fig. 2a and Fig. 2c) are simulated by 3-nodes plain strain solid elements, all other elements of the sub-models are simulated by 4-nodes plain strain solid elements, which are the same as 4-nodes plane42 elements with the plane strain option in ANSYS software. Since the sub-models are symmetric about the center line of the tunnel, only half of the sub-models are used to reduce the computational time.

The width and the depth of the sub-models are 80 m and 45 m respectively. The mesh size of the slab in Fig. 2(a), mat layer in Fig. 2(a), tunnel in Fig. 2(a) and Fig. 2(c) and near-field surrounding soil in Fig. 2(a) and Fig. 2(c) is between 0.1 m-0.625 m, which is dimensioned in detail in Fig. 2(a) and Fig. 2(c). The mesh size of the far-field soil is 0.625 m or 1.25 m, which is dimensioned in detail in Fig. 2(b) and Fig. 2(d).

The bottom and right boundary surfaces of the sub-models are modeled with the 2D viscous-elastic dynamic artificial absorbing boundary adopted in reference [30] to avoid the influence of reflected wave from boundary surfaces on the calculated results, and constrains are applied to all the outside nodes of absorbing boundary elements.

It is a crucial concern to reasonably transfer the forces generated by the 2D load generation

sub-models into equivalent forces used in the 2D wave propagation sub-models. Currently, there are two types of equivalent force transfer methods widely used in the 2D wave propagation sub-models. One method is according to the time history of a wheel-rail force. The equivalent force $P(t)$ can be written as follow.

$$P(t)=F(t)\times j/L \tag{1}$$

where $F(t)$ is the time history of a wheel-rail force generated by the 2D load generation sub-models; j is the number of wheels of the train; and L is the total length of train.

The other is according to the time history of fastening or steel spring forces averaged over certain characteristic length L_f, which is shown in Fig. 3(a). The expression of equivalent force $P(t)$ is as follow.

$$P(t)=\frac{\sum_{n=1}^{N} F_n(t)}{N} \tag{2}$$

where $F_n(t)$ is the time history of the n-th fastening force or steel spring force generated by the 2D load generation sub-models, and N is the total number of fasteners or steel springs within the characteristic length L_f.

Three types of characteristic lengths are considered. The first type is the spacing of fastener or steel spring. The second type is an integral multiple of the spacing of fastener or steel spring, and should be as close to the spacing between front and rear wheels of two bogies of two adjacent vehicles, as shown in Fig. 3(b). The third type is an integral multiple of the spacing of fastener or steel spring, and should be as close to the vehicle length, as shown in Fig. 3(c).

2.2 3D prediction models

3D simulation of train-track-tunnel-soil coupling dynamic, which considers the effect of moving train and 3D tunnel-soil interaction with all solid elements, is very time-consuming in time domain. In order to reduce the computational time and reflect the essential nature of 3D tunnel-soil interaction at the same time, a subway train-mixed 2D and 3D direct fixation track -tunnel-soil coupling dynamic model and a subway train-mixed 2D and 3D steel spring floating slab track -tunnel-soil coupling dynamic model, which consider the coupling interaction between all components of the whole system, the influence of random track irregularity, the 3D tunnel-soil interaction, and the effect of moving train,

are developed and used to predict the 3D responses of ground surface for underground direct fixation track and steel spring floating slab track respectively. As the models are symmetric about the central line of the tunnel, only half of the actual models are considered.

Each of 3D prediction models consists of four sub-models, namely, the subway train sub-model, the mixed 2D and 3D ballastless track -tunnel-soil sub-model, the wheel-rail interaction sub-model, and the track irregularity sub-model.The subway train sub-model is the same as that used in the 2D load generation sub-models, as shown in Fig. 1. The wheel-rail interaction sub-model and the track irregularity sub-model will be described in detail in Section 2.3 and 2.4 below respectively. The followings are the detailed descriptions of mixed 2D and 3D ballastless track-tunnel-soil sub-models, which are shown in Figs. 4(a)-(b) for underground direct fixation track and Figs. 4(c)-(d) for steel spring floating slab track, respectively.

The rail in Figs. 4(a)-(d) is simulated by 3D Bernoulli-Euler beam elements. The fastener in Figs. 4(a)-(d) is simulated by spring-damper elements. The slab, tunnel and soil in the middle part of Fig. 4(a) and Fig. 4(c), the mat layer in the middle part of Fig. 4(a), and the steel spring in the middle part of Fig. 4(c) are simulated by 8-node 3D solid elements, which are the same as 8-nodes solid45 elements in ANSYS software. The slab and tunnel in the two side parts of Fig. 4(a) and Fig. 4(c) are simulated by 3D Bernoulli-Euler beam elements. The mat layer in the two side parts of Fig. 4(a), the steel spring in the two side parts of Fig. 4(c) and the tunnel foundation in the two side parts of Fig. 4(a) and Fig. 4(c) are simulated by spring-damper elements.

The mesh size along the train-moving direction for the rail beam elements, slab beam elements, slab solid elements, tunnel beam elements, as well as mat layer solid elements for direct fixation track and steel spring solid elements for steel spring floating slab track, is 0.3125 m. The mesh size along the train-moving direction for the tunnel and soil solid elements of middle side(90 m) and two sides(30+30 m) , is 0.625 m and 1.25 m, respectively, as shown in Fig. 4(a) and Fig. 4(c).

The cross-section mesh size of the 3D models in Figs. 4(a)-(d) is the same as that of 2D wave propagation sub-models in Figs. 2(a)-(b). Each of the models consists of more than 1.5 million nodes with more than 4.5 million degree of freedoms.

All degree of freedoms of the bottom nodes of the tunnel foundation are constrained. Constraint equations are used to connect the tunnel beam elements and tunnel solid elements at the connecting

point between them. For soil solid elements, except the top boundary surface and symmetry surface, the other four boundary surfaces are modeled as the viscous-elastic dynamic artificial absorbing boundary adopted in reference [31] to avoid the influence of reflected wave from boundary surfaces on the calculated results, and constrains are applied to all the outside nodes of the four boundary surfaces.

2.3 Wheel-rail interaction sub-model

The wheel-rail interaction element is shown in Fig. 5. The contact point between the wheel and the rail is simulated by moving spring element. The relationship among wheel-rail contact force，wheel-rail contact stiffness, wheel displacement, rail displacement, and track irregularity is expressed as:

$$F(j,t) = K[Z_w(j,t) - Z_r(j,t) - \xi] \tag{3}$$

where $F(j,t)$ is the interaction force between the *j*-th wheel and rail at time *t*; K is equivalent linear spring stiffness between wheel and rail; $Z_w(j,t)$ is the *j*-th wheel displacement at time *t*; $Z_r(j,t)$ is the rail displacement under the *j*-th wheel at time *t*; and ξ is the irregularity of track under the *j*-th wheel at time *t* whose values can be obtained by the track irregularity model in Section 2.4.

The equivalent linear spring stiffness K is the contact stiffness under static wheel-rail contact force, which can be calculated according to Hertzian nonlinear contact expression [32].

2.4 Track irregularity sub-model

The medium-long as well as short wavelength random track irregularity is widely used in the railway traffic-induced environmental vibrations [12-13, 15, 21-23] and vehicle-track dynamics [32-37]. Their formation mechanism, measuring method, wavelength and spectrum expression are all different.

In order to reflect the actual track irregularity condition more accurately, both the short wavelength random irregularity of the track whose wavelength is between 0.02-1 m and the medium-long wavelength random irregularity of the track whose wavelength is between 1-80 m are considered in the 2D and 3D prediction models.

The Sato track irregularity spectrum and American class 6 track irregularity spectrum are adopted for the former and latter, respectively. The expression of Sato track irregularity spectrum [33] is as follow.

$$S(\Omega) = \frac{A}{\Omega^3} \tag{4}$$

where $S(\Omega)$ denotes the power spectral density; Ω denotes spatial frequency, rad/m; A denotes roughness constant, whose value is between 4.15×10^{-8} m·rad and 5.0×10^{-7} m·rad. According to reference [37], A is taken as 3.15×10^{-7} m·rad in this study. The expression of the America class 6 track irregularity spectrum can be found in reference [32], and is omitted to reduce the length of the paper.

The method described in reference [23] is used for the generation of sample waves in time series according to the expression of the power spectral density of track irregularity via superposition of simple random process with various statistical properties. The generated sample waves in time series according to the Sato track irregularity spectrum (Eq. (4)) and American class 6 track irregularity spectrum are shown in Fig. 6(a) and Fig. 6(b) respectively .The combined sample, as shown in Fig. 6(c), is generated by adding each amplitude of two samples whose coordinate is the same.

2.5 Determination of the equivalent stiffness of the tunnel foundation

The following procedures are used to determine the equivalent stiffness of the tunnel foundation.

(1) Use ANSYS Parametric Design Language to develop the 2D ballastless track-tunnel-soil sub-model in Fig. 1(a) or Fig. 1(b) and the 3D ballastless track-tunnel-soil sub-model of 3D prediction model in Fig. 4(a) or Fig. 4(c).

(2) Apply the train load to the 3D ballastless track-tunnel-soil sub-model, and obtain the maximum vertical displacement y of the tunnel.

(3) Assume three initial stiffness values for the tunnel foundation in 2D ballastless track-tunnel sub-model, namely, the first initial stiffness value k_1, whose value is 1×10^{6} N/m and less than the calculated equivalent stiffness, the second initial stiffness value k_2 , whose value is 1×10^{8} N/m and larger than the calculated equivalent stiffness. , and the third initial stiffness value k_3 , whose value is the average of k_1 and k_2.

(4) Apply the train load to the 2D ballastless track-tunnel sub-model with the foundation stiffness values k_1, k_2, and k_3, and obtain the maximum vertical displacements of the tunnel y_1, y_2, and y_3, respectively.

(5) Calculate the error between y and y_3. If the error between y and y_3 is less than 1×10^{-9} m, then the calculated equivalent stiffness is k_3. Otherwise, return to the procedure (4) and continue the

computation using the bisection iterative method until the relative error between y and y_3 is less than 1×10^{-9} m.

The proposed procedures are robust and the equivalent stiffness of the tunnel foundation can be obtained after 5-10 iterative cycles..

2.6 Establishment and solution of the equations of models

By using the principle of a stationary value of total potential energy of dynamic system presented by Zeng [38], also seeing reference [39], the vibration equation for the 2D and 3D prediction models can be derived. Because the establishment and solution of the equations of 2D prediction models are similar to those of 3D prediction models, only the establishment and solution of the equations of 3D prediction models are presented.

The equation of each of 3D prediction models can be written in matrix form as follow:

$$\begin{bmatrix} M_{vv} & 0 \\ 0 & M_{tt} \end{bmatrix} \begin{Bmatrix} \ddot{X}_v \\ \ddot{X}_t \end{Bmatrix} + \begin{bmatrix} C_{vv} & 0 \\ 0 & C_{tt} \end{bmatrix} \begin{Bmatrix} \dot{X}_v \\ \dot{X}_t \end{Bmatrix} + \begin{bmatrix} K_{vv} & 0 \\ 0 & K_{tt} \end{bmatrix} \begin{Bmatrix} X_v \\ X_t \end{Bmatrix} = \begin{Bmatrix} F_{vg} + F_{vi} \\ F_{ti} \end{Bmatrix} \tag{5}$$

where, $\ddot{X}_v$, $\dot{X}_v$, and X_v denote the acceleration, velocity, and displacement vectors of the subway train sub-model, respectively; $\ddot{X}_t$, $\dot{X}_t$, and X_t denote the acceleration, velocity, and displacement vectors of the 3D ballastless track-tunnel-soil sub-model, respectively; M_{vv}, C_{vv}, and K_{vv} denote the mass, damping, and stiffness matrices of the subway train sub-model, respectively; M_{tt}, C_{tt}, and K_{tt} denote the mass, damping, and stiffness matrices of the 3D ballastless track-tunnel-soil sub-model, respectively; F_{vg} denotes the gravity sub-load vector of the subway train sub-model; F_{vi} and F_{ti} denote the sub-load vector of the wheel-rail interaction forces on subway train sub-model and 3D ballastless track-tunnel-soil sub-model, respectively.

The following procedures can be used to obtain the dynamic responses of these models.

(1) At time t=0, a static analysis is performed and the solution is used as initial condition for latter dynamic analysis.

(2) When t >0, the dynamic responses for each time step can be obtained using Newmark-β step-by-step integration method [40] combined with preconditioned conjugate gradient solving techniques [41].

3 Calculation parameters

Unless otherwise mentioned, the following parameters are used in the numerical simulation afterwards.

The B-type subway train consists of six identical vehicles, and the parameters of vehicle are shown in Table 1.

Two types of tracks, namely, steel spring floating slab track and direct fixation track, are considered, and the parameters of the tracks are shown in Table 2. Except the last three parameters in Table 2 are for direct fixation and steel spring floating slab track respectively, all other parameters are for both tracks. It should be mentioned that the stiffness of mat layer and steel spring in Table 2 will be used to determine the equivalent elastic modulus of the mat layer and steel spring when they are required to be modeled as 3D solid elements.

A single-track bored tunnel is shown in Fig. 7. The center of the tunnel is 13m below ground surface. The internal radius and wall thickness of the tunnel are 3.0 m and 0.4 m, respectively. The dynamic elastic modulus E_t, the Poisson's ratio ν_t and the density ρ_t of the tunnel are 32.5 GPa, 0.2 and 2500 kg/m^3, respectively. The dynamic elastic modulus E_s, the Poisson's ratio ν_s and the density ρ_s of the soil are 150 MPa, 0.3 and 2000 kg/m^3, respectively.

The initial position of the front wheel of the train is 40 m behind the mid-section of the models. The train moves 194 m forward along the track at a speed of 20 m/s. When the train-moving process is completed, the position of the last wheel of the train is 40 m ahead the mid-section of the models.

In numerical simulation for each case, each time step Δt of 0.0025 s is adopted, i.e., the running distance of train during each time step is 0.05m, and total time steps of 3880 are used.

Seven observational points O1, O2, . . ., O7 of ground surface at mid-section of the models at distances of 0-60 m with 10 m intervals from the central line of the tunnel, as shown in Fig. 7, are chosen as the output points for the calculated results.

4 Validation of 3D prediction models

To verify the correctness of the 3D prediction models, the 3D responses of ground surface calculated by the 3D prediction model for underground direct fixation track are used to compare with those from in situ measurements.

In situ vibration measurements were carried out in the section of direct fixation track between the Dongdan station and Jianguomen station on subway line 1 of Beijing [42]. Sensors were fixed on the ground surface at distances of 20 m, 40 m, 80 m, and 100 m from the observation point of ground surface just above the center of the underground tunnel to measure the vibrations induced by passage of the metro train, and the corresponding measured acceleration vibration levels are 71.6 dB, 61.5 dB, 56.2 dB, and 56.6 dB.

Corresponding numerical simulation is conducted by the self-developed program, which is coded by the MATLAB programming language. The calculated acceleration vibration levels of ground surface at distances of 20 m and 40 m are 70.9 dB and 63.3 dB, respectively. Although the results calculated and measured in situ are not in accordance with each other totally, they are still in agreement to some extent. Considering the discrepancy between the random irregularity of track used in this study and that in situ, as well as other uncertainties involved, the discrepancy of the results can be accepted.

5 Case studies

In order to conduct a comparative study on 2D and 3D responses of ground surface with various 2D and 3D prediction models due to underground railway traffic for underground direct fixation track and steel spring floating slab track, as well as to study the applicability of 2D environmental vibration prediction models with various equivalent forces for these two types of underground tracks, ten cases are studied. The first five cases listed in Table 3 and the latter five cases listed in Table 4 are for underground direct fixation track and steel spring floating slab track, respectively. 3D prediction models are used in the Case 1 and Case 6, and 2D prediction models are used in the other eight cases.

Three types of equivalent forces are considered for Cases 2-5 and Cases 7-10. The first and second equivalent force are, respectively, the equivalent fastening force and the equivalent steel spring force averaged over characteristic length, and the last equivalent force is the equivalent wheel-rail force averaged over the whole length of train.

Three types of characteristic lengths for averaging the fastening forces or the steel spring forces are considered. The first one is the spacing of fastener or steel spring, whose value is 0.625 m for averaging fastening force or 1.875 m for averaging steel spring force. The second one is according to the spacing between front and rear wheel of two bogies of two adjacent vehicles, whose value is 6.25 m which is 10 times integral multiple of fastening spacing for averaging fastening forces, or 7.5 m which

is 4 times integral multiple of steel spacing for averaging steel spring forces. And the third one is according to the vehicle length, whose value is 19.375 m which is 31 times integral multiple of fastening spacing for averaging fastening forces, or 18.75 m which is 10 times integral multiple of steel spacing for averaging steel spring forces.

The parameters of train, track, tunnel and soil for ten cases are the same as those in Section 3. The random track irregularity for ten cases is shown in Fig. 6(c). Besides the vibration acceleration, vibration acceleration level (VAL) considering frequency weighting [43] is used as another index for evaluating environmental vibration.

The equivalent forces, which are calculated by the 2D load generation sub-models, and will be used as the acting forces for 2D wave propagation sub-models for Cases 2-5 and Cases 7-10, are plotted in Figs. 8(a)-(h), respectively. The acceleration histories and corresponding frequency distributions of O1 and O5 for Cases 1-10 are plotted in Figs. 9-18, respectively. The VALs of seven observational points, which are calculated according to reference [43], are listed in Table 5 and Table 6 for Cases 1-5 and Cases 6-10, respectively.

From the simulation results, the following points can be obtained.

(1) By using the subway train-mixed 2D and 3D ballastless track-tunnel-soil models, where the two side parts of the ballastless track-tunnel-soil interaction are simulated by Bernoulli-Euler beam elements and spring-damper elements, and the middle part of the ballastless track-tunnel-soil interaction is simulated by 3D solid elements, the computational time of 3D responses can be significantly reduced due to the significantly reduced number of 3D solid elements in the model. And the subway train-ballastless track-tunnel-soil coupling dynamic problem which takes the 3D tunnel-soil interaction and moving train along track with irregularity into account can now be implemented in a personal computer with finite element method.

(2) From Figs. 8(a)-(c) and Figs. 8(e)-(g), it can be seen that characteristic length has great influence on the amplitude and frequency of equivalent fastening force and equivalent steel spring force. The general rule is that the longer the characteristic length is, the smaller the amplitude of equivalent force is and the higher the frequency of equivalent force is. For example, the maximum peak value of equivalent force averaged over 0.625 m characteristic length is more than 40 kN as shown in Fig. 8(a)，while the maximum peak value of equivalent force averaged over 19.375 m characteristic

length is less than 20 kN as shown in Fig. 8(c). The reason is that the fastening forces and steel spring forces which are within the characteristic length and will be used to calculate the equivalent force have different phases, so the the amplitude and frequency of the averaged equivalent forces according to different characteristic lengths vary greatly. It is vital to choose a suitable equivalent force transfer method to improve the prediction accuracy of environmental vibration with 2D prediction models.

(3) From Figs. 10-12 and Figs. 15-17, it can be found that the amplitude and frequency of 2D responses of ground surface excited by different equivalent fastening forces or steel spring forces differ greatly due to different amplitude and frequency of different equivalent fastening forces and steel spring forces. With the increase of averaged characteristic length of exciting force, the amplitude of 2D responses of ground surface tends to become smaller, while the frequency of 2D responses of ground surface tends to become higher. For example, the maximum peak value in Fig. 10(a) is near 0.2m/s^2, while the maximum peak value in Fig. 12(a) is less than 0.06 m/s^2, the dominant frequency range in Fig. 10(a) is between 0 and 10 Hz, the dominant frequency range in Fig. 12(a) is between 60 and 100 Hz.

(4) For underground direct fixation track, by comparing the 3D simulation results of environmental vibration with 2D simulation results of environmental vibration in Table 5 and Figs. 9-12, it can be found that the 2D responses of ground surface calculated with the equivalent wheel-rail force agree better with the 3D responses of ground surface than that calculated by other types of equivalent forces. The equivalent wheel-rail force is more suitable for environmental vibration prediction for underground direct fixation track than other types of equivalent forces. However, from Table 5, it can also be found that the VAL difference at O1 and O7 for 3D responses is 18.2 dB, while the VAL difference at O1 and O7 for 2D responses is less than 13 dB, the 3D responses of ground surface decrease more rapidly with the distance away from the central line of the tunnel than the 2D responses of ground surface for underground direct fixation track. So it is difficult to obtain accurate prediction results for all observational points on ground surface for underground direct fixation track with 2D prediction models.

(5) For underground steel spring floating slab track, by comparing the 3D simulation results of environmental vibration with 2D simulation results of environmental vibration in Table 6 and Figs. 14-18, it can be found that the 2D responses of ground surface calculated with the equivalent steel spring force averaged over a vehicle length agree better with the 3D responses of ground surface than

that calculated by other types of equivalent forces. The equivalent steel spring force averaged over a vehicle length is more suitable for environmental vibration prediction than other types of equivalent forces. The discrepancy between VAL of 3D responses of ground surface and VAL of 2D responses of ground surface calculated with the equivalent steel spring averaged over a vehicle length is less than 1 dB for underground steel spring floating slab track. The 2D simulation results calculated by the equivalent steel spring force averaged over a vehicle length are accurate enough for evaluating the overall influence of environmental vibration on human beings. However, by comparing Fig. 14 for Case 6 with Fig. 17 for Case 9, we can find that there are some discrepancies between the frequency content of 2D responses for Case 9 and 3D responses for Case 6. 3D responses for Case 6 contains more high-frequency vibrations, while 2D responses for Case 9 contains more low-frequency vibrations, especially the frequency content below 5 HZ, which is mainly caused by the static moving load of train. So the results of 2D simulation are not suitable for the evaluation of sensitive instruments which are very sensitive to certain frequency range.

(6) The computational time for each case calculated by 2D prediction models and that calculated by 3D prediction models are, respectively, less than 3 minutes and 27 hours in a personal computer with Intel I5 3470 CPU and 16 GB random memory. the computational time for each case calculated by 2D prediction models is more than 500 times less than that calculated by 3D prediction models. Due to the much higher computational efficiency, the relatively lower accuracy of simulation result, and easy-to-use feature, 2D prediction models are suitable for the track-soil-tunnel interaction problems where the qualitative behavior, rather than the quantitative behavior, is of primary concern. 2D prediction models are especially favored by most practicing engineers during the early-stage assessment of environmental vibration and determination of which type of vibration isolation measure should be taken.

(7) Although the computational time using 3D prediction models is much longer, they can give more accurate simulation results than 2D prediction models, and they are applicable to a much wider range of complex practical engineering problems. 3D prediction models are required for absolute prediction during final-stage assessment of environmental vibration.

6 Conclusions

In this study, the 2D responses of ground surface calculated by 2D prediction models with various

equivalent forces are compared to the 3D responses calculated by 3D prediction models for both underground direct fixation track and steel spring floating slab track. From the comparison of results, the following conclusions can be drawn.

(a) The amplitude and frequency distribution of 2D responses of ground surface excited by the equivalent fastening force or equivalent steel spring force averaged with various characteristic lengths differ greatly. With the increase of averaged characteristic lengths of exciting force, the amplitude of 2D responses of ground surface tends to become smaller, while the frequency of 2D responses of ground surface tends to become higher. It is vital to choose a suitable equivalent force transfer method for 2D prediction models to improve the prediction accuracy of environmental vibration.

(b) For underground direct fixation track, the 2D prediction model with the equivalent wheel-rail force is more suitable for prediction of environmental vibration. However, the 2D responses of ground surface decrease more slowly with distance away from the central line of the tunnel than the 3D responses of ground surface, so it is difficult to obtain accurate 2D responses for all observation points on ground surface.

(c) For underground steel spring floating slab track, the 2D prediction model with the equivalent steel spring force averaged over a vehicle length is more suitable for evaluating the influence of environmental vibration on human beings. However, there are some discrepancies among the frequency content of 2D and 3D responses of ground surface, so the 2D prediction model is not suitable for assessing the influence of environmental vibration on sensitive instruments which are very sensitive to certain frequency range.

(d) the simulation time for each case calculated by 2D prediction models is more than 500 times less than that calculated by 3D prediction models. However, the accuracy of 2D prediction models is relatively lower. 2D prediction models are suitable for the track-soil-tunnel interaction problems where the qualitative behavior is of primary concern. 3D prediction models are required for absolute prediction during final-stage assessment of environmental vibration due to their high accuracy and applicability to all complex conditions.

Acknowledgements

The works described in this paper are supported by National Natural Science Foundation of China (Nos.51178469 and 51078360) and the National Science Joint High Speed Railway Foundation of

China (No. U1334203), as well as the State Scholarship Fund of China Scholarship Council (No. 201208430112).

References

[1] Chua KH, Lo KW, Balendra T. Building response due to subway train traffic. J Geotech Eng-ASCE 1995; 121(11): 747-754.

[2] Tadeu AJB, Kausel E, Vrettos C. Scattering of waves by subterranean structures via the boundary element method. Soil Dyn Earthq Eng 1996;15(6):387-397.

[3] Yang YB, Hung HH, Hsu LC. Ground vibrations due to underground trains considering soil-tunnel interaction. Interact Multi Mech–An Int J 2008; 1(1): 157-175.

[4] Nejati HR, Ahmadi M, Hashemolhosseini H. Numerical analysis of ground surface vibration induced by underground train movement. Tunn Undergr Sp Tech 2012; 29: 1-9.

[5] Nejati HR, Ahmadi M, Hashemolhosseini H, Hayati M. Probabilistic analysis of ground surface vibration due to train movement, a case study on Tehran metro line 4. Geotech Geol Eng 2012; 30(5): 1137-1146.

[6] Jones S, Hunt H. Predicting surface vibration from underground railways through inhomogeneous soil. J Sound Vib 2012; 331(9): 2055-2069.

[7] Godinho L, Amado-Mendes P, Pereira A, Soares Jr D. A coupled MFS-FEM model for 2-D dynamic soil-structure interaction in the frequency domain . Comput Struct 2013; 129: 74-85.

[8] Sun XJ, Liu WN, Zhai H, Ding DY, Guo JP. Vibration effects of metro trains on sensitive instruments and the study of the mitigation measures. Tunn Undergr Sp Tech 2006; 21(3): 299-299.

[9] Huang JK, Shi ZF. Attenuation zones of periodic pile barriers and its application in vibration reduction for plane waves . J Sound Vib 2013; 332(19): 4423-4439.

[10] Yang YB, Hung HH. A 2.5 D finite/infinite element approach for modelling visco‐elastic bodies subjected to moving loads. Int J Numer Meth Eng 2001;51(11): 1317-1336.

[11] Yang YB, Hung HH. Soil vibrations caused by underground moving trains. J Geotechnol Geoenviron Eng ASCE 2008;134(11): 1633-1644.

[12] Hung HH, Chen GH, Yang YB. Effect of railway roughness on soil vibrations due to moving trains by 2.5 D finite/infinite element approach. Eng Struct 2013; 57: 254-266.

[13] Sheng X, Jones CJC, Thompson DJ. Prediction of ground vibration from trains using the wavenumber finite and boundary element methods . J Sound Vib 2006; 293(3): 575-586.

[14] François S, Schevenels M, Galvín P, Lombaert G, Degrande G. A 2.5 D coupled FE-BE methodology for the dynamic interaction between longitudinally invariant structures and a layered halfspace. Comput Method Appl M 2010; 199(23): 1536-1548.

[15] Galvin P, François S, Schevenels M, Bongini E, Degrande G, Lombaert G. A 2.5 D coupled FE-BE model for the prediction of railway induced vibrations . Soil Dyn Earthq Eng 2010; 30(12): 1500-1512.

[16] Hussein MFM, Hunt HEM. A numerical model for calculating vibration from a railway tunnel embedded in a full-space. J Sound Vib 2007; 305(3): 401-431.

[17] Müller K, Grundmann H, Lenz S. Nonlinear interaction between a moving vehicle and a plate elastically mounted on a tunnel. J Sound Vib 2008; 310(3): 558-586.

[18] Bian XC, Jin WF, Jiang HG. Ground-borne vibrations due to dynamic loadings from moving trains in subway tunnels . J Zhejiang Univ Sci A 2012;13(11): 870-876.

[19] Degrande G, Clouteau D, Othman R, Arnst M, Chebli H, Klein R, et al. A numerical model for ground-borne vibrations from underground railway traffic based on a periodic finite element-boundary element formulation . J Sound Vib 2006; 293(3): 645-666.

[20] Chebli H, Othman R, Clouteau D, Arnst M, Degrande G. 3D periodic BE-FE model for various transportation structures interacting with soil . Comput Geotech 2008; 35(1): 22-32.

[21] Gupta S, Stanus Y, Lombaert G, Degrande G. Influence of tunnel and soil parameters on vibrations from underground railways . J Sound Vib 2009; 327(1): 70-91.

[22] Gupta S, Degrande G. Modelling of continuous and discontinuous floating slab tracks in a tunnel using a periodic approach. J Sound Vib 2010; 329(8): 1101-1125.

[23] Gupta S, Liu WF, Degrande G, Lombaert G, Liu WN. Prediction of vibrations induced by underground railway traffic in Beijing. J Sound Vib 2008; 310(3): 608-630.

[24] Wolf S. Potential low frequency ground vibration (< 6.3 Hz) impacts from underground LRT operations . J Sound Vib 2003; 267(3): 651-661.

[25] Ma M, Markine V, Liu WN, Yuan Y, Zhang F. Metro train-induced vibrations on historic buildings in Chengdu, China. J Zhejiang Univ Sci A 2011; 12(10): 782-793.

[26] Gardien W, Stuit HG. Modelling of soil vibrations from railway tunnels. J Sound Vib 2003; 267(3): 605-619.

[27] Yaseri A, Bazyar MH, Hataf N. 3D coupled scaled boundary finite-element/finite-element analysis of

ground vibrations induced by underground train movement. Comput Geotech 2014; 60: 1-8.

[28] Saitoh T, Hirose S. 3-D Analysis of the Influence of a Pile on Underground Induced Vibrations Using the Boundary Element Method . J Mech Syst Transp Logis 2010; 3(1): 259-270.

[29] Andersen L, Jones CJC. Coupled boundary and finite element analysis of vibration from railway tunnels-a comparison of two-and three-dimensional models. J Sound Vib 2006; 293(3): 611-625.

[30] Liu JB, Gu Y, Du YX. Consistent viscous-spring artificial boundaries and viscous-spring boundary elements. Chin J Geotech Eng 2006; 28(9): 1070-1075 [in Chinese].

[31] Gu Y, Liu JB, Du YX. 3D consistent viscous-spring artificial boundary and viscous-spring boundary element. Eng Mech 2007; 24(12): 31-38 [in Chinese].

[32] Lei X, Noda NA. Analyses of dynamic response of vehicle and track coupling system with random irregularity of track vertical profile. J Sound Vib 2002; 258(1): 147-165.

[33] Sato Y. Study on high-frequency vibrations in track operated with high-speed trains. Quarterly Report of Railway Technical Research Institute (Rpt No. 1013-76). 1977; 18(3):109-114.

[34] Nielsen JCO. High-frequency vertical wheel–rail contact forces-validation of a prediction model by field testing. Wear 2008; 265(9): 1465-1471.

[35] Hardy AEJ, Jones RRK, Turner S. The influence of real-world rail head roughness on railway noise prediction. J Sound Vib 2006; 293(3): 965-974.

[36] Xu QY. Influence of short-wave random irregularity on the dynamic characteristics of train-slab track-bridge system. Chin Civ Eng J 2011; 44(10): 132-137 [in Chinese].

[37] Xu ZS. Prediction and control of wheel/ rail noise for rail transit [Ph.D. Thesis]. Cheng Du: Southwest Jiaotong University 2004 [in Chinese].

[38] Zeng QY. The Principle of Total Potential Energy with Stationary Value in Elastic System Dynamics. J Huazhong Univ Sci Technolo Sci 2000; 28(1):1-3 [in Chinese].

[39] Lou P. Finite element analysis for train-track-bridge interaction system. Arch Appl Mech 2007; 77(10): 707-728.

[40] Newmark NM. A method of computation for structural dynamics, J Eng Mech Div (ASCE) 1959; 85(3):67-94.

[41] Ju SH, Kung KJS. Mass types, element orders and solution schemes for the Richards equation. Comput Geosci 1997; 23(2): 175-187.

[42] Liu WF, Liu WN, Yuan Y, Li KF, Wu ZZ. In-situ measurements of and analysis on environmental

effects of vibrations induced by passage of Metro trains and vehicles on the road. J Chin Railway Sci 2013; 35(5): 80-84 [in Chinese].

[43] International Organization for Standardization. Mechanical vibration and shock-Evaluation of human exposure to whole-body vibration-Part 1: General requirements, ISO-2631-1. International Standards Organization, 1997.

Figure captions

Fig. 1 Schematic of the load generation sub-models of 2D prediction models for (a) underground direct fixation track and (b) underground steel spring floating slab track

Fig. 2 Schematic of the wave propagation sub-models of 2D prediction model. (a) is for the sub-model where the acting force is the averaged wheel-rail force or averaged fastening force ,and (c) is for the sub-model where the acting force is the averaged steel spring force. (b) and (d) are the detailed mesh size of the far-field soil for (a) and (c) respectively.

Fig. 3 Schematic of characteristic length Lf. (a) is the fastening or steel spring forces within the characteristic length for averaging, (b) is for the determination of the second type of characteristic length, and (c) is for the determination of the third type of characteristic length

Fig. 4 Overall graph (a) and enlarged graph(b) of direct fixation track-tunnel-soil sub-model of 3D prediction model, overall graph(c) and enlarged graph(d) of steel spring floating slab track-tunnel-soil sub-model of 3D prediction model

Fig. 5 Wheel-rail interaction element

Fig. 6 Samples of the short wavelength random track irregularity (a), medium-long wavelength random track irregularity (b), and combined random track irregularity (c)

Fig. 7 Position of tunnel and observational points O1-O7 at ground surface (O1 is just above the center of the tunnel)

Fig. 8 Equivalent force history, (a) for Case 2, (b) for Case 3, (c) for Case 4, (d) for Case 5, (e) for Case 7, (f) for Case 8 , (g) for Case 9, and (h) for Case 10

Fig. 9 Time history (a) and frequency distribution (b) of acceleration at O1, time history (c) and frequency distribution (d) of acceleration at O5 for case 1

Fig. 10 Time history (a) and frequency distribution (b) of acceleration at O1, time history (c) and frequency distribution (d) of acceleration at O5 for case 2

Fig. 11 Time history (a) and frequency distribution (b) of acceleration at O1, time history (c) and frequency distribution (d) of acceleration at O5 for case 3

Fig. 12 Time history (a) and frequency distribution (b) of acceleration at O1, time history (c) and frequency distribution (d) of acceleration at O5 for case 4

Fig. 13 Time history (a) and frequency distribution (b) of acceleration at O1, time history (c) and frequency distribution (d) of acceleration at O5 for case 5

Fig. 14 Time history (a) and frequency distribution (b) of acceleration at O1, time history (c) and frequency distribution (d) of acceleration at O5 for case 6

Fig. 15 Time history (a) and frequency distribution (b) of acceleration at O1, time history (c) and frequency distribution (d) of acceleration at O5 for case 7

Fig. 16 Time history (a) and frequency distribution (b) of acceleration at O1, time history (c) and frequency distribution (d) of acceleration at O5 for case 8

Fig. 17 Time history (a) and frequency distribution (b) of acceleration at O1, time history (c) and frequency

distribution (d) of acceleration at O5 for case 9

Fig. 18 Time history (a) and frequency distribution (b) of acceleration at O1, time history (c) and frequency distribution (d) of acceleration at O5 for case 10

Figures

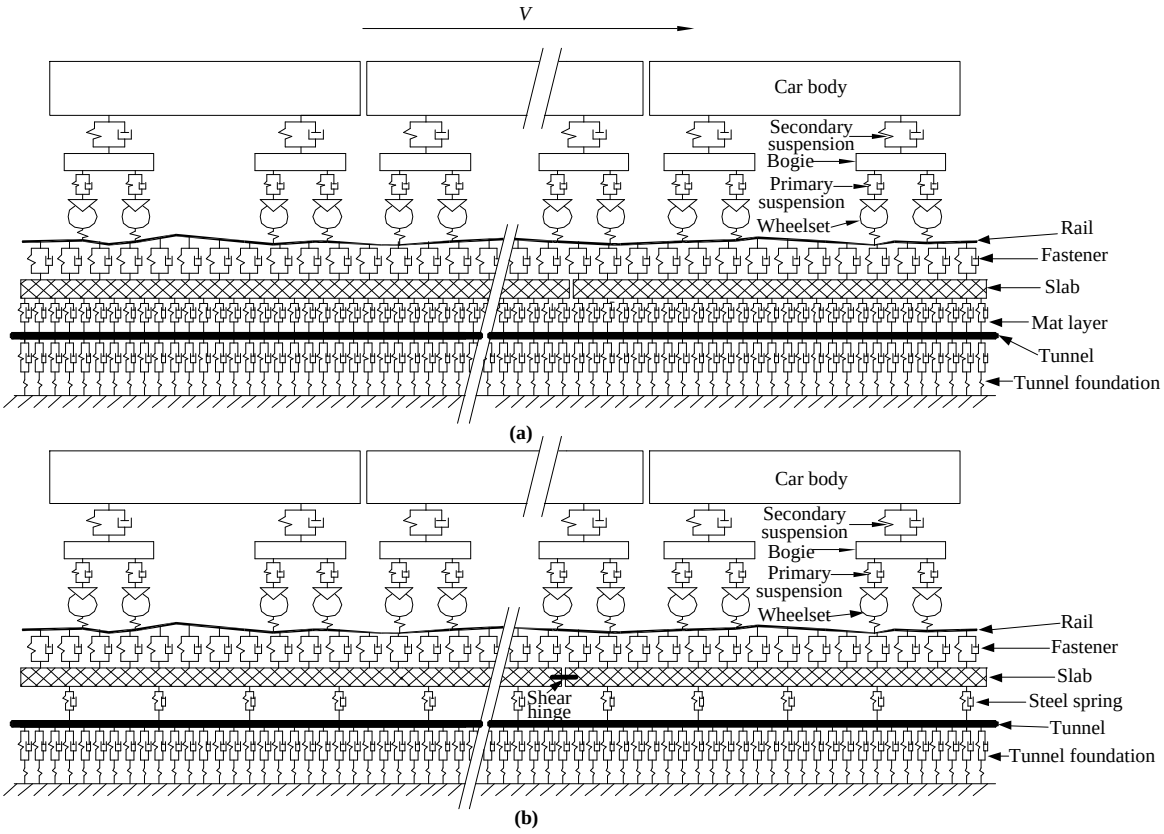

Fig. 1 Schematic of the load generation sub-models of 2D prediction models for (a) underground direct fixation track and (b) underground steel spring floating slab track

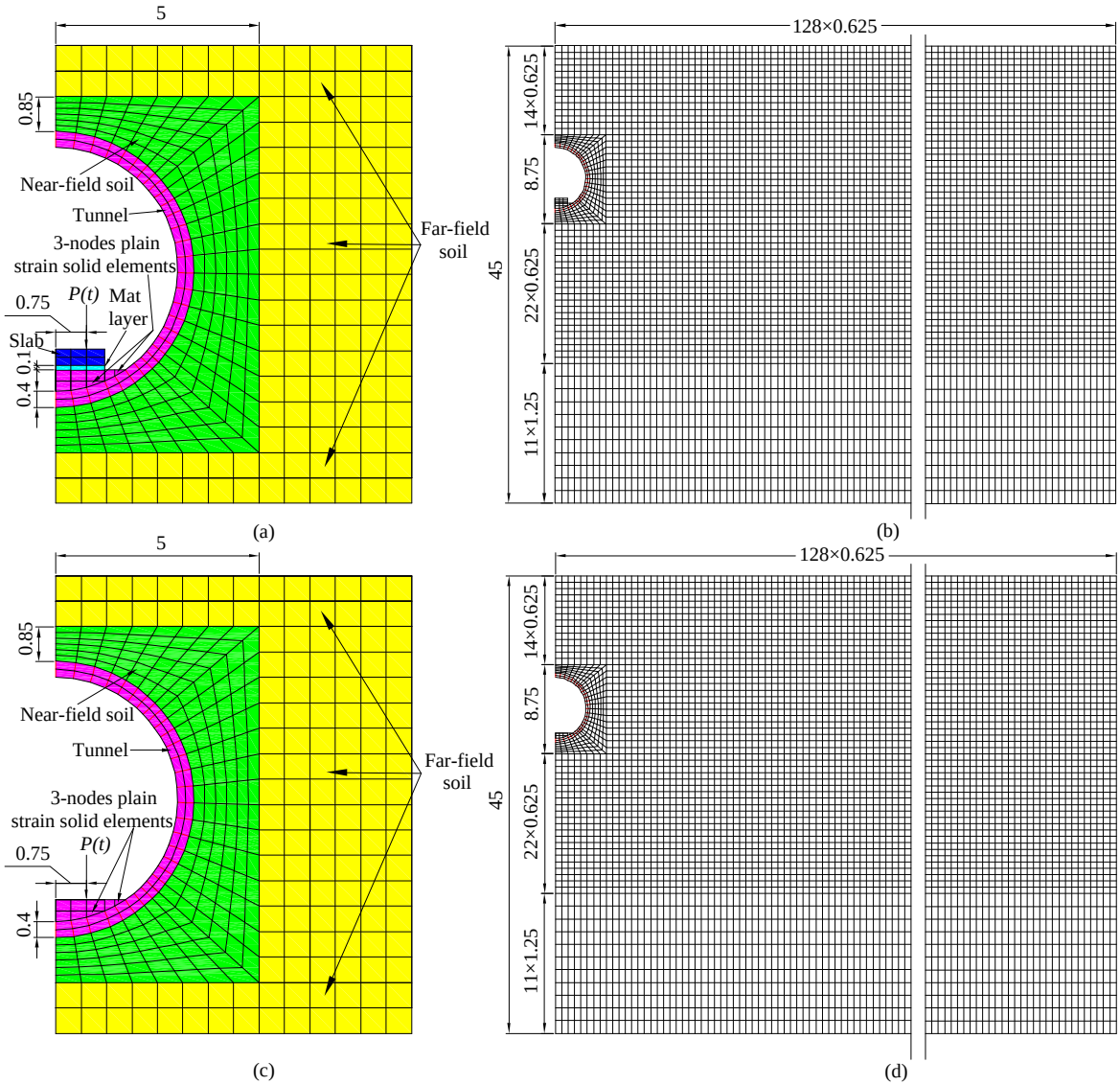

Fig. 2 Schematic of the wave propagation sub-models of 2D prediction model. (a) is for the sub-model where the acting force is the averaged wheel-rail force or averaged fastening force ,and (c) is for the sub-model where the acting force is the averaged steel spring force. (b) and (d) are the detailed mesh size of the far-field soil for (a) and (c) respectively. The unit for length in Fig. 2 is m.

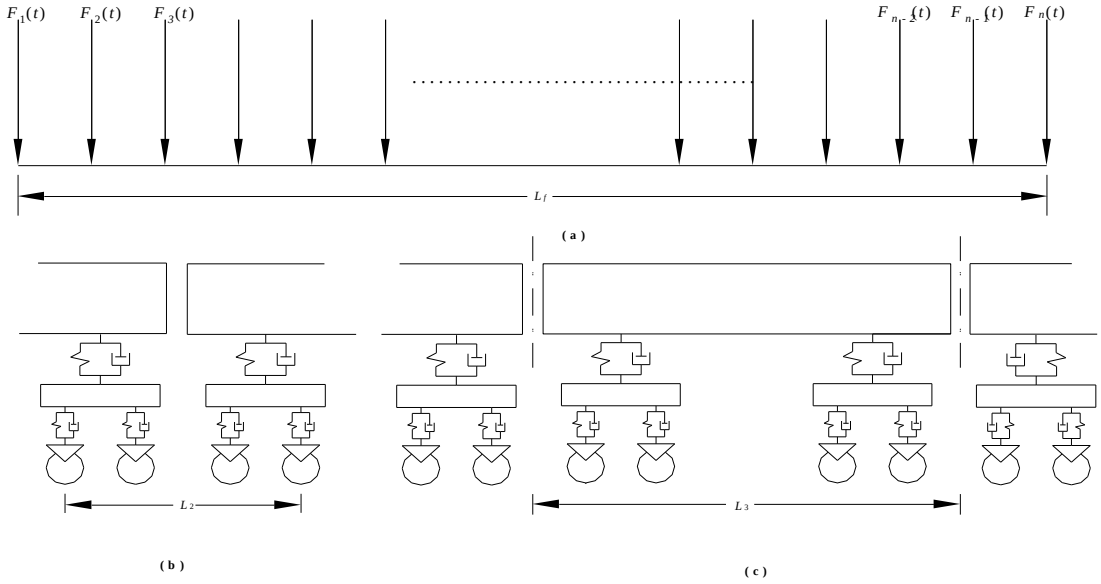

Fig. 3 Schematic of characteristic length L_f. (a) is the fastening or steel spring forces within the characteristic length for averaging, (b) is for the determination of the second type of characteristic length, and (c) is for the determination of the third type of characteristic length

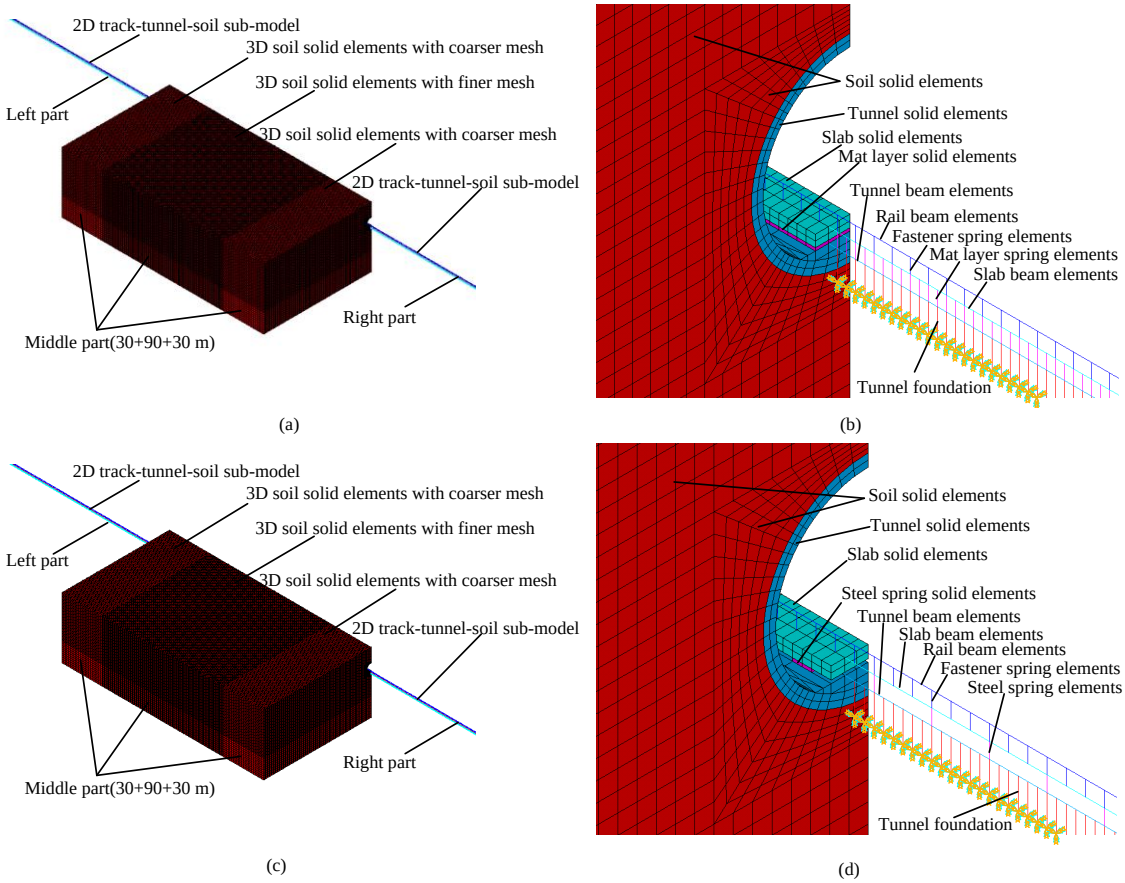

Fig. 4 Overall graph (a) and enlarged graph(b) of direct fixation track-tunnel-soil sub-model of 3D prediction model, overall graph(c) and enlarged graph(d) of steel spring floating slab track-tunnel-soil sub-model of 3D prediction model

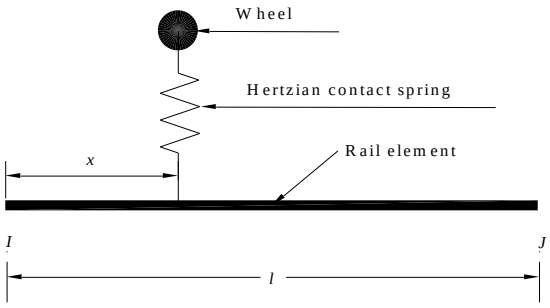

Fig. 5 Wheel-rail interaction element

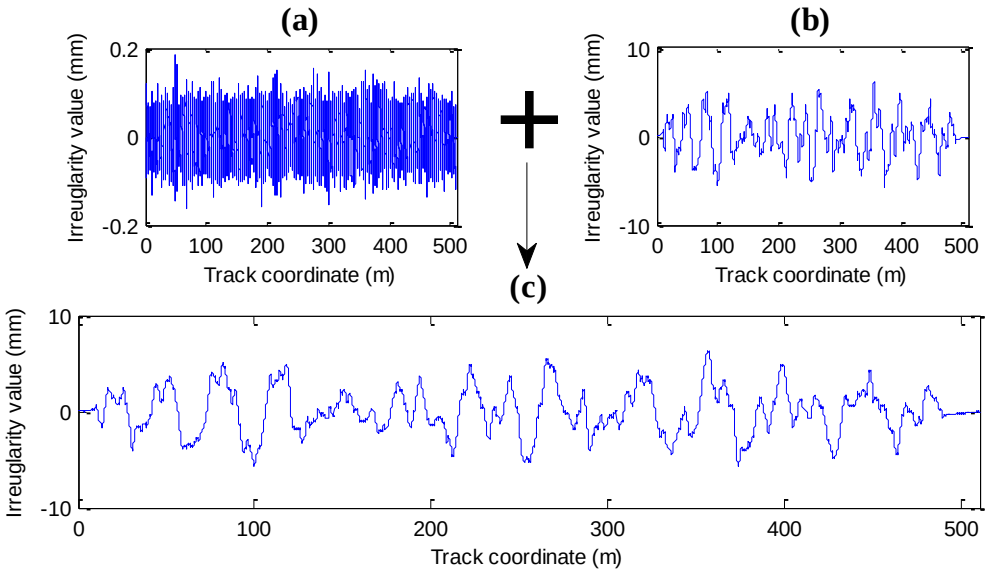

Fig. 6 Samples of the short wavelength random track irregularity (a), medium-long wavelength random track irregularity (b), and combined random track irregularity (c)

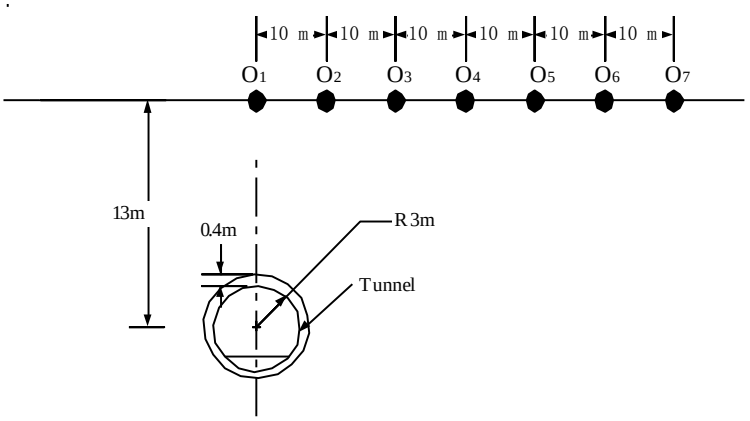

Fig. 7 Position of tunnel and observational points O1-O7 at ground surface (O1 is just above the center of the tunnel)

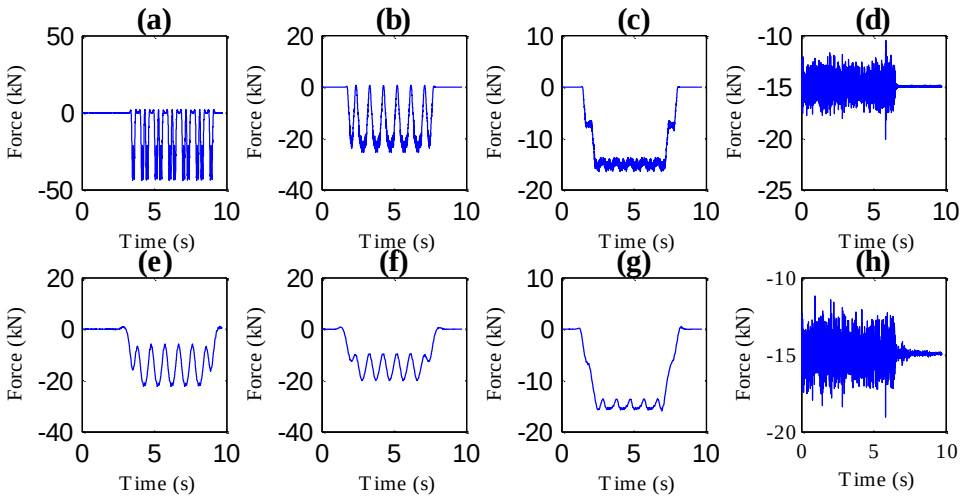

Fig. 8 Equivalent force history, (a) for Case 2, (b) for Case 3, (c) for Case 4, (d) for Case 5, (e) for Case 7, (f) for Case 8, (g) for Case 9, and (h) for Case 10

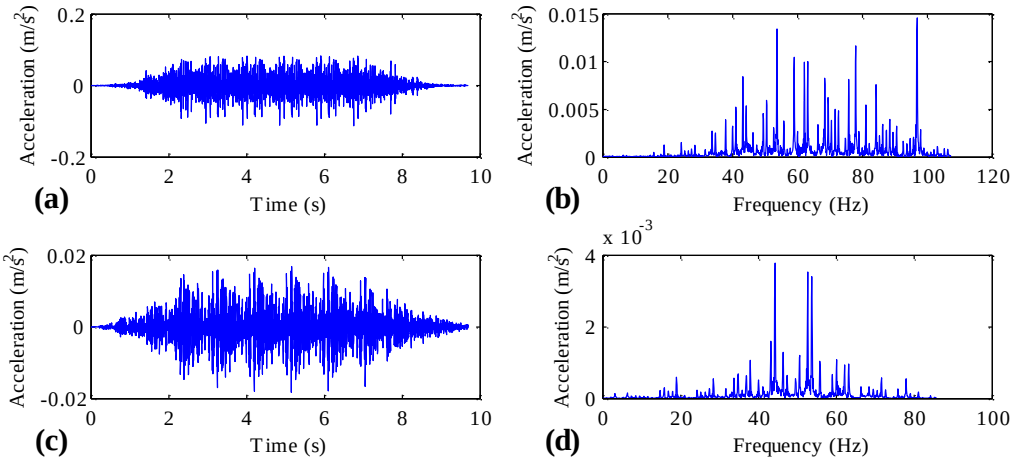

Fig. 9 Time history (a) and frequency distribution (b) of acceleration at O1, time history (c) and frequency distribution (d) of acceleration at O5 for case 1

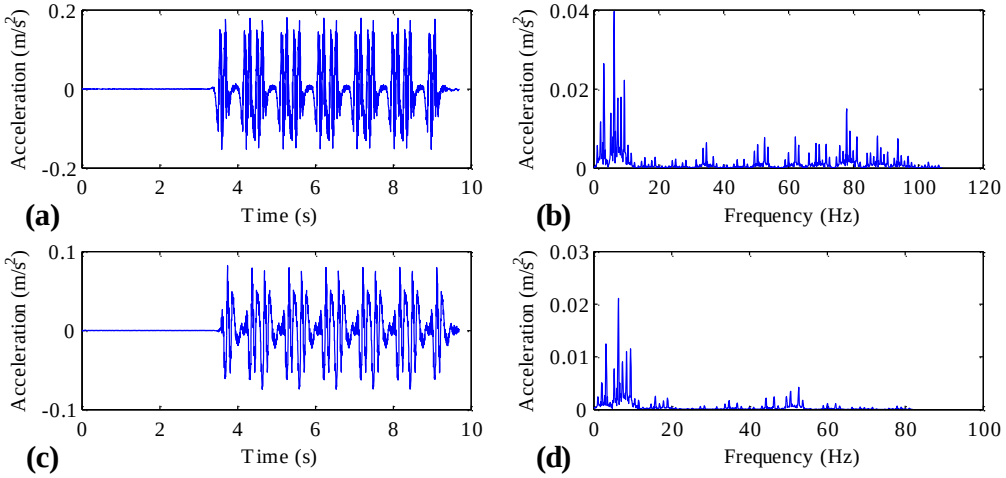

Fig. 10 Time history (a) and frequency distribution (b) of acceleration at O1, time history (c) and frequency distribution (d) of acceleration at O5 for case 2

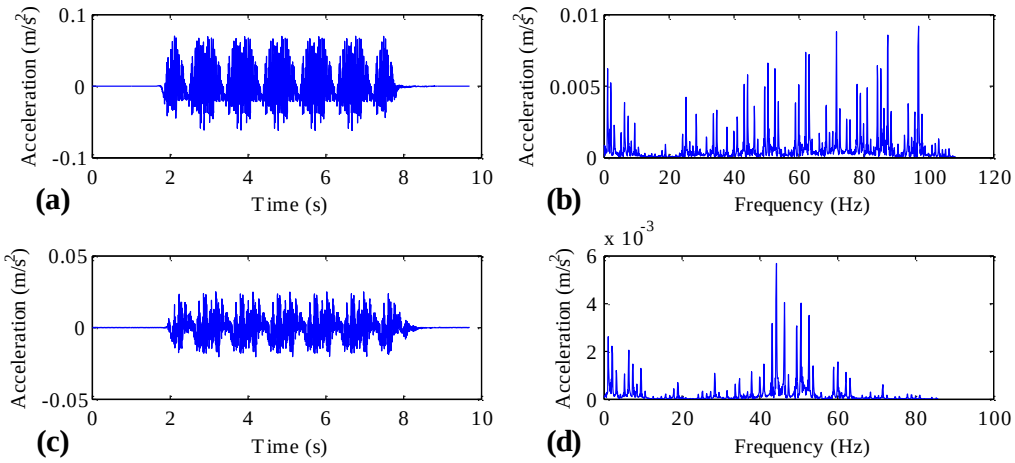

Fig. 11 Time history (a) and frequency distribution (b) of acceleration at O1, time history (c) and frequency distribution (d) of acceleration at O5 for case 3

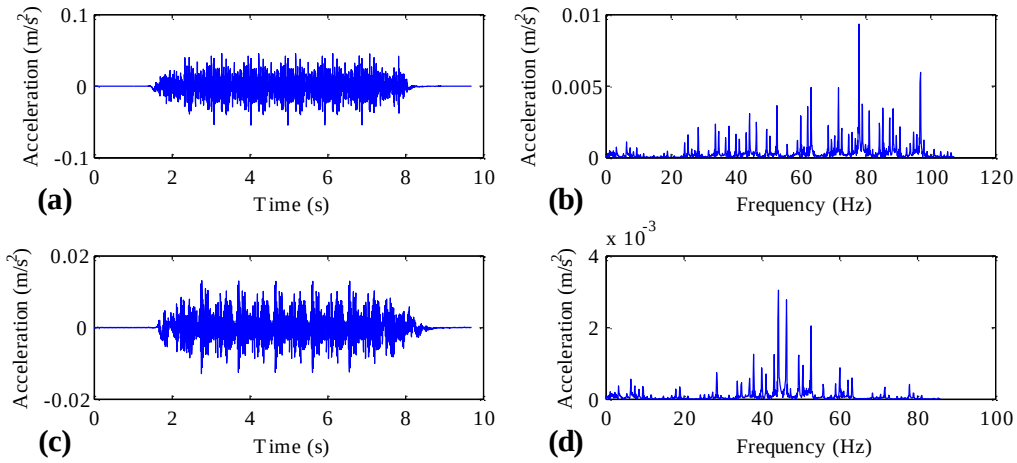

Fig. 12 Time history (a) and frequency distribution (b) of acceleration at O1, time history (c) and frequency distribution (d) of acceleration at O5 for case 4

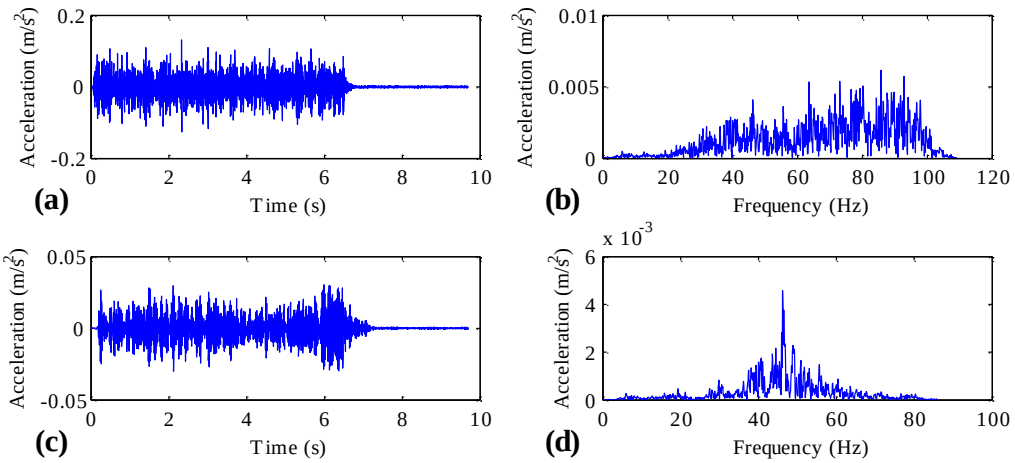

Fig. 13 Time history (a) and frequency distribution (b) of acceleration at O1, time history (c) and frequency distribution (d) of acceleration at O5 for case 5

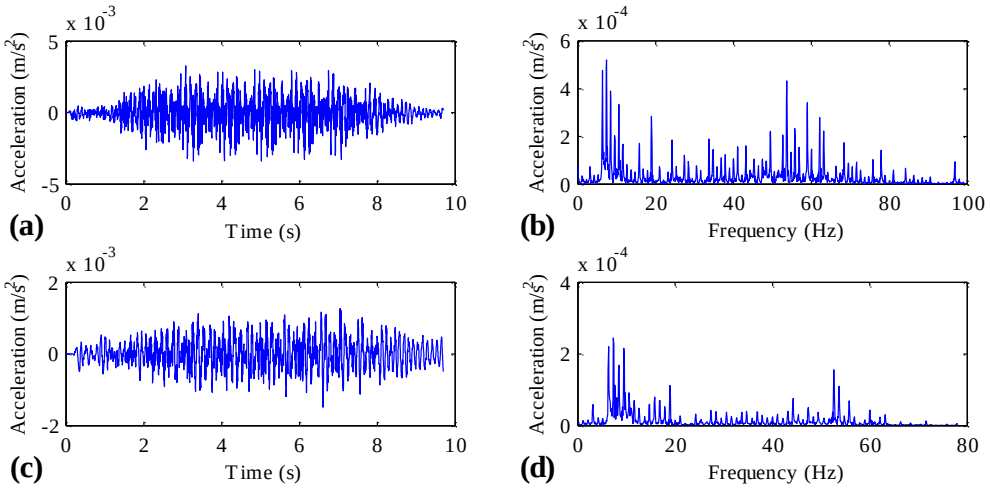

Fig. 14 Time history (a) and frequency distribution (b) of acceleration at O1, time history (c) and frequency distribution (d) of acceleration at O5 for case 6

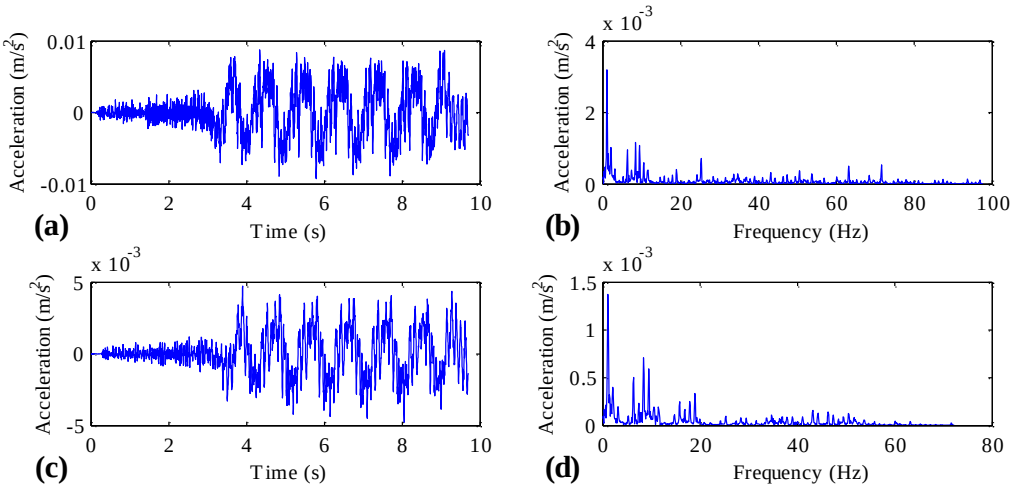

Fig. 15 Time history (a) and frequency distribution (b) of acceleration at O1, time history (c) and frequency distribution (d) of acceleration at O5 for case 7

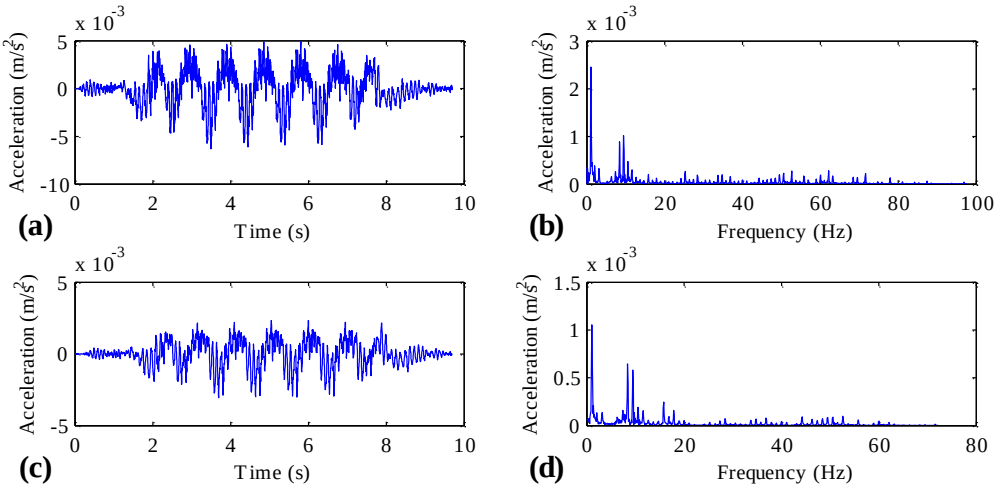

Fig. 16 Time history (a) and frequency distribution (b) of acceleration at O1, time history (c) and frequency distribution (d) of acceleration at O5 for case 8

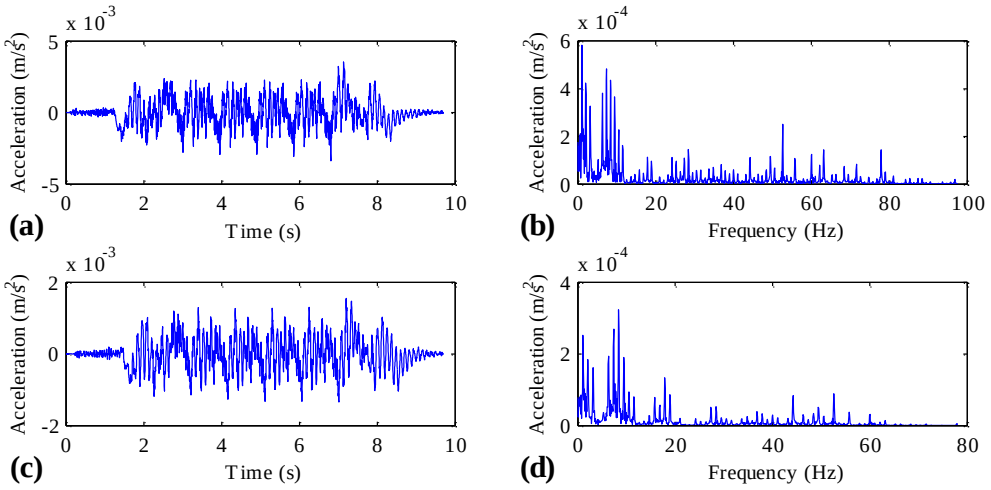

Fig. 17 Time history (a) and frequency distribution (b) of acceleration at O1, time history (c) and frequency distribution (d) of acceleration at O5 for case 9

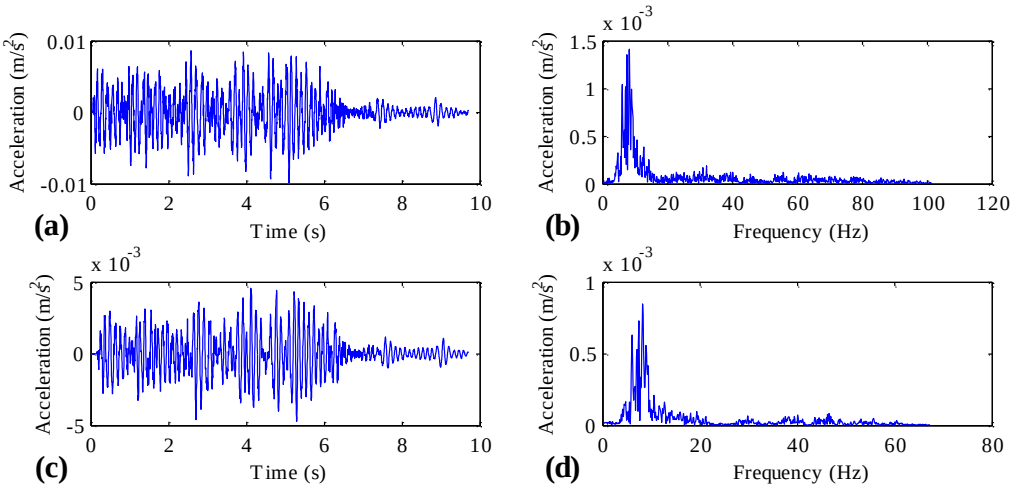

Fig. 18 Time history (a) and frequency distribution (b) of acceleration at O1, time history (c) and frequency distribution (d) of acceleration at O5 for case 10

Tables

Table 1 Parameters of vehicle

Parameters	Notation	Unit	Value
Mass of car body	M_c	kg	43000
Mass of bogie	M_t	kg	3600
Mass of wheelset	M_w	kg	1900
Moment of inertia of car body	I_c	kg.m^2	1400000
Moment of inertia of bogie	I_t	kg.m^2	2320
Vertical stiffness of primary suspension	K_1	N/m	1400000
Vertical damping of primary suspension	C_1	N.m/s	30000
Vertical stiffness of secondary suspension	K_2	N/m	580000
Vertical damping of secondary suspension	C_2	N.m/s	50000
Half-distance between two bogies of a vehicle	L_c	m	6.3
Half-distance between wheel-sets of a bogie	L_t	m	1.15
Full length of vehicle	L	m	19
Contact stiffness of wheel-rail	K	MN/m	970

Table 2 Parameters of track

Parameters	Notation	Unit	Value
Mass of rail per unit length	M_r	kg/m	60.64
Area of rail section	A_r	m^2	77.45×10^{-4}
Elastic modulus of rail	E_r	GPa	210
Inertia moment of rail	I_r	m^4	3217×10^{-8}
Poisson's ratio of rail	ν_r	-	0.27
Spacing of rail pad	l_r	m	0.625
Rail pad stiffness	K_p	MN/m	50
Rail pad damping	C_p	kN.m/s	20
Slab height	h_s	m	0.4
Slab width	l_s	m	2.5
Young's modulus of slab	E_t	GPa	35
Density of slab	ρ_t	kg/m^3	2500
Poisson's ratio of slab	ν_{ss}	-	0.2
Stiffness of mat layer under the slab for direct fixation track	K_{p1}	MPa/m	1000
Stiffness of steel spring under the slab for steel spring floating slab track	K_{p2}	kN/m	6900
Spacing between adjacent steel springs for steel spring floating slab track	L_{p2}	m	1.875

Table 3 Load cases for underground direct fixation track

Case	Prediction model types	Characteristic length for force averaging (m)	Force type for force averaging
1	3D	-	-
2	2D	0.625	fastening
3	2D	6.25	fastening
4	2D	19.375	fastening
5	2D	-	wheel-rail

Table 4 Load cases for underground steel spring floating slab track

Case	Prediction model types	Characteristic length for force averaging (m)	Force type for force averaging
6	3D	-	-
7	2D	1.875	steel spring
8	2D	7.5	steel spring
9	2D	18.75	steel spring
10	2D	-	Wheel-rail

Table 5 Vibration acceleration level of ground surface for underground direct fixation track

Observational point	Case 1	Case 2	Case 3	Case 4	Case 5
O1	75.2	94.0	77.3	69.7	75.1
O2	72.6	88.0	77.5	71.2	77.7
O3	70.9	87.4	75.2	68.5	75.1
O4	66.7	89.3	73.2	65.6	70.5
O5	63.3	88.5	71.0	62.8	68.2
O6	58.3	86.1	68.2	58.4	65.3
O7	57.0	84.9	67.0	57.7	62.0

Note: the unit is dB.

Table 6 Vibration acceleration level of ground surface for underground steel spring floating slab track

Observational point	Case 6	Case 7	Case 8	Case 9	Case 10
O1	57.8	67.0	63.2	58.2	68.9
O2	52.5	63.9	59.6	53.2	60.8
O3	51.9	62.8	59.6	53.0	63.2
O4	53.2	62.7	59.6	54.1	64.6
O5	51.8	61.2	58.2	53.2	63.5
O6	49.2	58.2	54.8	49.9	60.3
O7	47.9	56.0	51.6	48.0	58.1

Note: the unit is dB.